



## OPEN ACCESS

## EDITED BY

Mohamed F. Hamoda,  
Kuwait University, Kuwait

## REVIEWED BY

Megat Ahmad Kamal Megat Hanafiah,  
Universiti Teknologi Mara, Malaysia  
Hani Abu-Qdais,  
Jordan University of Science and Technology,  
Jordan  
Maria Laura Tummino,  
National Research Council of Italy (CNR), Italy

## \*CORRESPONDENCE

Brigitte Helmreich,  
✉ b.helmreich@tum.de

RECEIVED 01 December 2023

ACCEPTED 11 January 2024

PUBLISHED 31 January 2024

## CITATION

Strebel A, Behringer M, Hilbig H, Machner A and Helmreich B (2024), Anionic azo dyes and their removal from textile wastewater through adsorption by various adsorbents: a critical review.

*Front. Environ. Eng.* 3:1347981.

doi: 10.3389/fenv.2024.1347981

## COPYRIGHT

© 2024 Strebel, Behringer, Hilbig, Machner and Helmreich. This is an open-access article distributed under the terms of the [Creative Commons Attribution License \(CC BY\)](https://creativecommons.org/licenses/by/4.0/). The use, distribution or reproduction in other forums is permitted, provided the original author(s) and the copyright owner(s) are credited and that the original publication in this journal is cited, in accordance with accepted academic practice. No use, distribution or reproduction is permitted which does not comply with these terms.

# Anionic azo dyes and their removal from textile wastewater through adsorption by various adsorbents: a critical review

Annika Strebel<sup>1</sup>, Martin Behringer<sup>2</sup>, Harald Hilbig<sup>2</sup>, Alisa Machner<sup>2</sup> and Brigitte Helmreich<sup>1\*</sup>

<sup>1</sup>Chair of Urban Water Systems Engineering, TUM School of Engineering and Design, Technical University of Munich, Garching, Germany, <sup>2</sup>Mineral Construction Materials, TUM School of Engineering and Design, Technical University of Munich, Munich, Germany

The review aimed to identify differences and similarities in the adsorption process of five azo dyes [congo red (CR), reactive black 5 (RB5), methyl orange (MO), orange II (OII), and methyl red (MR)] on natural materials, biosorbents, industrial and agricultural waste, or biomass, which are alternatives of costly activated carbon and are locally available. The azo dyes were characterized and compared based on their molecular structure and weight, water solubility, acid dissociation constant, n-octanol-water partition coefficient, and maximum absorbance. RB5 and CR are diazo dyes, whereas MO, OII, and MR are mono-azo dyes. MO, OII, and MR are anionic acid dyes, RB5 is an anionic reactive dye, and CR is an anionic direct dye. CR, RB5, MR, and OII molecules contain one or more sulfonate functional group(s), but MR does not. We performed a literature review based on the following parameters: initial dye concentration, adsorbent dosage, pH, temperature, isotherm, kinetic models, thermodynamic parameters, and synergetic or competitive interactions. The azo dyes tended to adsorb best in an acidic medium and at higher temperatures. The initial dye concentration and adsorbent dosage studies indicated the importance of using an appropriate amount of adsorbent dosage for an effective removal. The studies tended to follow the Langmuir isotherm and kinetic pseudo-second-order model. Most adsorption processes were endothermic and spontaneous, leading to an increase in randomness at the solid-liquid interface. These results indicate similarities between the adsorption process of the five azo dyes. Relevant adsorption mechanisms in azo dye adsorption processes were assumed to be electrostatic forces, hydrogen bonding, and  $\pi$ - $\pi$  interactions, among others. Nevertheless, the focus of the studies lies more on the development and characterization of adsorbent materials, not on the study of influences from the matrix "industrial wastewater". Therefore, more research is needed to develop adsorption units for application in textile industries.

## KEYWORDS

pollution, industrial wastewater, dyes, wastewater treatment, adsorption

## 1 Introduction

Many industrial processes, such as textile dyeing, paper printing, and the production of food or cosmetics, use azo dyes. From these, the textile industry is responsible for releasing a large quantity of azo dyes in wastewater and—if not adequately treated—discharges into the aquatic environment (Wong et al., 2019).

Correspondingly, about 50,000 tons/year of dyes are dumped into the environment (Dihom et al., 2022). Globally, it is estimated that textile production is responsible for about 20% of water pollution (Mani and Bharagava, 2018). This contamination mainly affects regions of textile industry hubs, such as India and Bangladesh, where water stress is already high. Southern and Central Asia, for example, registered high levels of water scarcity at over 75% in 2019, where the contamination of freshwater from untreated textile wastewater further threatens local ecosystems and deepens existing inequalities (Pan et al., 2021; OHCHR, 2022; UN, 2022).

Azo dyes are the most important class of synthetic textile dyes, accounting for over 60%–70% of all commercial dyes, and do not exist naturally in the environment (Berradi et al., 2019). They are widely used due to their readily synthesized varieties in chemical structure, their straightforward application methods, and their cost-effectiveness (Chudgar, 2000). While the complex structure of azo dyes gives them an advantage in application, this causes problems in removing them from wastewater (Wong et al., 2019).

Due to their specific features, azo dyes are not or hardly biodegradable and resistant to light, heat, and oxidizing agents, which makes it difficult to remove them in wastewater treatment plants (Wong et al., 2019; Lai et al., 2020). After discharge, untreated azo dye-containing wastewater accumulating in natural water bodies can be highly toxic and develop carcinogenic and mutagenic properties for human and aquatic life (Du et al., 2014; Lai et al., 2020).

Conventional biological wastewater treatment methods (aerobic and anaerobic) have often been proven inefficient for azo dye removal (Saad et al., 2010) because the process is not carried out under optimal conditions (Didier de Vasconcelos et al., 2021). For sufficient azo dye removal, a combination of an anaerobic step, which is responsible for discoloration by breaking azo bonds, and an aerobic step, which promotes an efficient removal of organic compounds, is necessary (Didier de Vasconcelos et al., 2021). Different enhanced treatment options are available, e.g., chemical methods (Coagulation/flocculation, Fenton oxidation, ozonation, photocatalytic or sonocatalytic oxidation, radiolysis), and physical methods (membrane filtration and adsorption) (Brillas and Martínez-Huitle, 2015; Wang F. et al., 2022; Dihom et al., 2022). Considering chemical methods, high costs of chemicals and reagents, large amounts of sludge (e.g., for coagulation/flocculation and Fenton oxidation), and problems faced during handling and disposal of wastes are drawbacks. Membrane filtration is a promising technology but has high operating costs and produces a concentrate which cannot be treated (Pang and Abdullah, 2013; Wang X. et al., 2022). In contrast, adsorption is a promising technology for the removal of azo dyes from wastewater because of its high efficiency, low cost, simplicity, high capacity, and ease of up-scaling (Tanyildizi, 2011; Yilmaz et al., 2016; Saleh and Al-Absi, 2017; Wang X. et al., 2022). For adsorption a large number of materials, such as activated carbon, polymeric resins, agricultural and industrial by-products (e.g., peat, bentonite, chitin, silica, and fly ash) are available (Wang X. et al., 2022). Some review articles were written, for example, on the adsorption of anionic or cationic azo dyes on agricultural solid waste (e.g., Salleh et al., 2011; Afroze and Sen, 2018; Birniwa et al., 2022; Haque et al., 2022). Adsorption does not degrade azo dyes but accumulates them onto the surface of the adsorbent. However, a prerequisite for applying materials as adsorbents is that they are produced with reproducible

quality and can best be regenerated and reused. It should be noted that regeneration is not possible, additional waste product is generated, and other costs are incurred.

The adsorption process of azo dyes is complex and depends on their individual physical and chemical characteristics including pore size, surface area, and pore volume and functional groups (Al-Amrani et al., 2022; Haque et al., 2022). Additionally, other physiochemical parameters, including modifier coverage, adsorbent dosage, temperature, contact time, initial dye concentration, pH, and agitation speed influence the adsorption process (Al-Amrani et al., 2022).

The focus of this paper is the discussion of adsorption studies of azo dye removal with adsorbents replacing costly activated carbon with more economical and locally available adsorbents with good adsorption performance. Understanding and maximizing the physical and chemical interactions at the molecular level involved in adsorption is vital for choosing or developing an appropriate adsorbent for treating azo-dye-containing wastewater (Pan et al., 2021; Li et al., 2022). Furthermore, textile wastewater can contain multiple types of azo dyes, and an adsorbent should ideally be able to remove them all. Most review papers about azo dye adsorption focus on a specific adsorbent material or adsorbate. This review aims to systematically compare adsorption behavior and interactions between diverse azo dyes and different kinds of adsorbents to critically reveal differences or similarities in their adsorption processes.

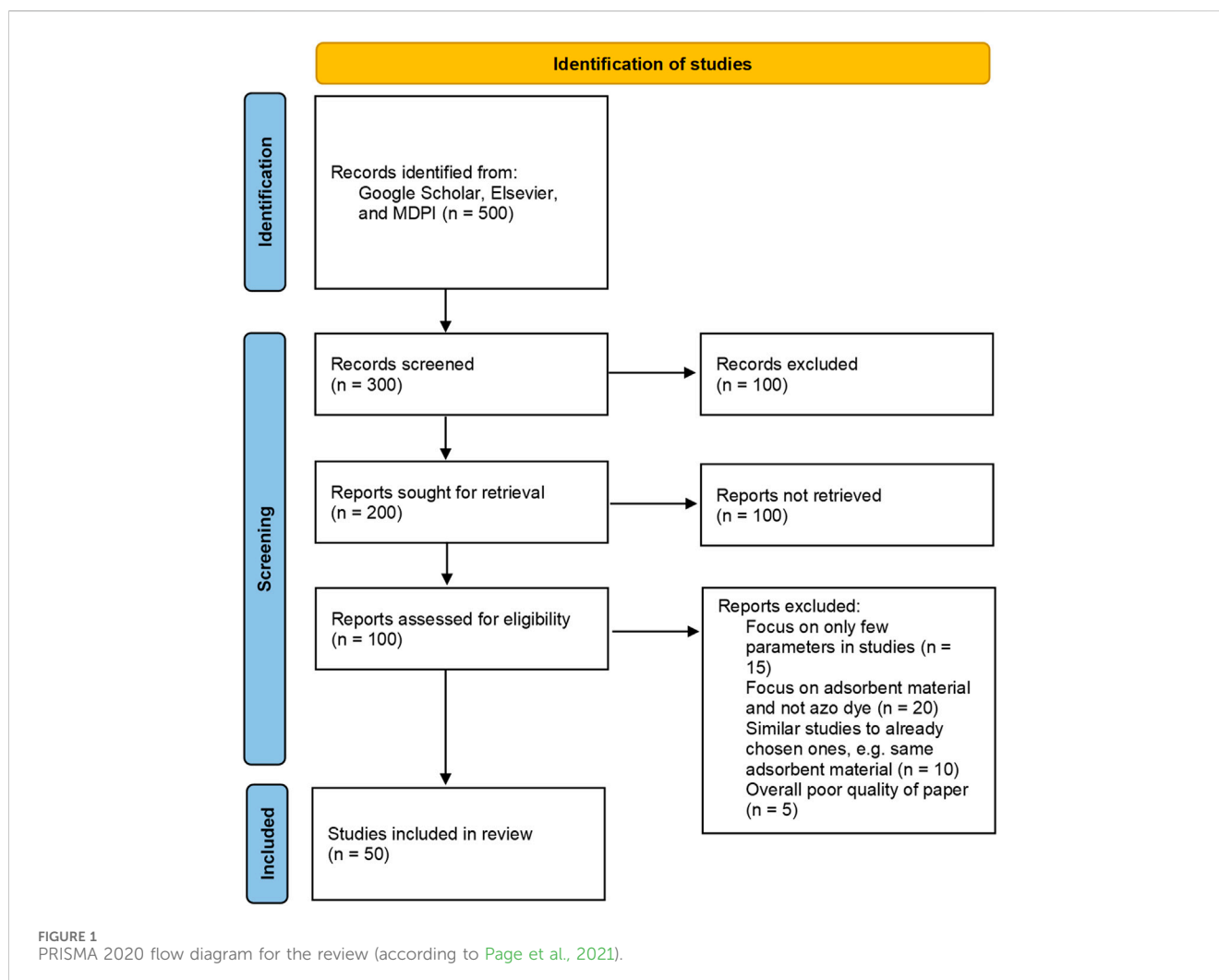
Therefore, this review characterizes five widely applied azo dyes, namely, congo red (CR), reactive black 5 (RB5), methyl orange (MO), orange II (OII), and methyl red (MR). We have chosen them based on their wide application in the textile industry, their structural behavior, difficulty removing them from wastewater, and the problems they cause for ecosystems and humans. The dyes are described and compared based on molecular structure and weight, water solubility, acid dissociation constant ( $pK_a$ ), n-octanol-water partition coefficient ( $\log K_{OW}$ ), and maximum absorbance ( $\lambda_{max}$ ). Moreover, we present an overview of the results and parameters of different adsorption studies of the above-mentioned azo dyes. For the review, 50 papers, with 66 studies, were identified and revised in detail. The effects of initial dye concentration, adsorbent dosage, pH, and temperature on adsorption are analyzed, as well as the isotherm and kinetic models, thermodynamic parameters, and synergetic or competitive interactions between different dyes.

Based on that, the objective is to answer the following research question:

- 1) Which adsorbents are available besides activated carbon with good adsorption performance?
- 2) Can general recommendations be given concerning parameters that affect their adsorption capacity and removal rate and available models?

## 2 Methodology

This study is based on the characterization and literature review of adsorption studies of the five azo dyes CR, RB5, MO, OII, and MR. We characterized and compared the dyes based on the following



parameters: molecular formula, molecular structure, molecular weight, water solubility,  $pK_a$ ,  $\log K_{OW}$ , and  $\lambda_{max}$  value.

We identified peer-reviewed papers published between 2002 and 2022 studying the adsorption of the above-mentioned azo dyes via Google Scholar, MDPI, and Elsevier. We selected the documents based on the intention to include diverse adsorbents and papers from various researchers from different countries, especially countries with big textile industries (see also Figure 1). Ten papers were selected for each of the five azo dyes and reviewed in detail according to a pre-defined set of parameters.

The following parameters are relevant based on their well-known importance and impact on adsorption processes: initial dye concentration, adsorbent dosage, pH, temperature, isotherm, thermodynamic parameters, and competitive or synergetic interactions with other dyes. Based on the results, adsorption mechanisms and interactions, which might occur during an adsorption process between an azo dye and an adsorbent, were proposed. The strengths and weaknesses of the investigated studies were also briefly mentioned. If information from the written text and available graphs or tables was contradictory, we used the information from graphs and tables.

Some papers tested more than one azo dye and adsorbent in their work. Finally, this resulted in the review of 11 articles with

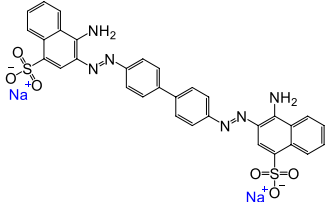
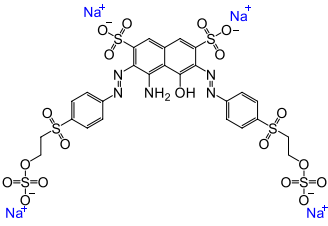
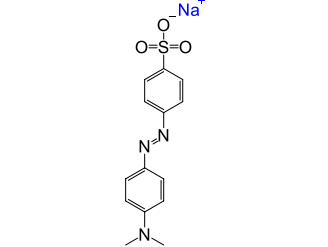
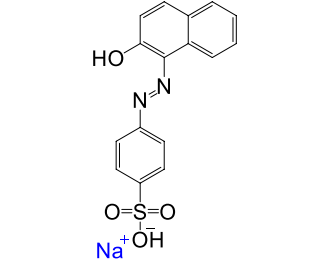
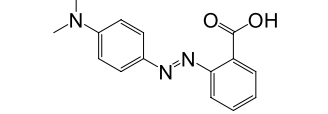
14 different studies for CR, 11 papers with 16 various studies for RB5, 13 articles with 15 various studies for MO, ten papers with 11 various studies for OII, and ten papers with ten different studies for MR. We analyzed the data using Microsoft Excel since a statistical analysis would require more studies.

### 3 Azo dyes characteristics

Generally, azo dyes can be classified according to their dissociation in an aqueous solution as anionic (acid, direct and reactive) dyes, cationic (basic) dyes, and nonionic (disperse) dyes (Eren and Acar, 2006; Munagapati et al., 2018). Due to their chemical structure, azo dyes are highly stable and hardly biodegradable; some are even carcinogenic and mutagenic (Chen et al., 2010; Du et al., 2014). Hence, they pose ecological and toxicological risks for aquatic life and human beings if discharged into receiving water bodies (Chen et al., 2010; Du et al., 2014; Zheng et al., 2019). Due to its chromophoric functional group, the azo bond linkage is primarily responsible for the color. It makes them highly stable owing to their complex aromatic rings and covalent azo bonds.

Several factors affect the adsorption process, including the adsorbate properties. Anionic azo dyes have different numbers of

TABLE 1 Overview of various characteristics and the structures of CR, RB5, MO, OII, and MR.

Azo dye	Molecular formula	Structure	Molecular weight (g/mol)	Dye Class/Chromophore	pK <sub>a</sub>	log K <sub>OW</sub>	λ <sub>max</sub> (nm) <sup>j</sup>	Water solubility at 20°C
CR	C <sub>32</sub> H <sub>22</sub> N <sub>6</sub> Na <sub>2</sub> O <sub>6</sub> S <sub>2</sub>		696.7	Direct/Diazo	4.1 <sup>a</sup>	2.63 <sup>g</sup> /3.57 <sup>f</sup>	495–501	25 g/L <sup>a</sup>
RB5	C <sub>26</sub> H <sub>21</sub> N <sub>5</sub> Na <sub>4</sub> O <sub>19</sub> S <sub>6</sub>		991.8	Reactive/Diazo	3.8 and 6.9 <sup>b</sup> / 2.89 <sup>i</sup>	< - 4.34 <sup>a, 1</sup>	590–603	550 g/L <sup>a</sup> / 551 g/L <sup>1</sup>
MO	C <sub>14</sub> H <sub>14</sub> N <sub>3</sub> NaO <sub>3</sub> S		327.3	Acid/Monoazo	3.46 <sup>c</sup> / k/3.2 <sup>n</sup>	-0.66 <sup>g</sup> / 0.0758 to 3.14 <sup>h</sup> /3.91 <sup>c</sup>	463–506	5 g/L <sup>a</sup> /1.39 x 10 <sup>-4</sup> to 3.63 mol/L <sup>g</sup> / 0.0153 mol/L <sup>c</sup>
OII	C <sub>16</sub> H <sub>11</sub> N <sub>2</sub> NaO <sub>4</sub> S		350.3	Acid/Monoazo	1 <sup>d, m</sup> and 10.6 <sup>d, n</sup> / 11.4 <sup>m</sup>	-0.95 <sup>a</sup> / 0.560 to 2.95 <sup>h</sup>	482–497	27 g/L <sup>a</sup> or 70 g/ L <sup>g</sup> /2.43 x 10 <sup>-5</sup> to 1.24 mol/L <sup>h</sup>
MR	C <sub>15</sub> H <sub>15</sub> N <sub>3</sub> O <sub>2</sub>		269.3	Acid/Monoazo	5.1 <sup>e</sup> / 2.88 <sup>n</sup>	3.83 <sup>a</sup> / 3.34 to 4.91 <sup>i</sup>	410–526	2.5 g/L <sup>a</sup> /2.13 x 10 <sup>-6</sup> to 4.36 mol/L <sup>1</sup>

<sup>a</sup>values extracted from respective Sigma Aldrich and Carl Roth safety data sheets (Sigma Aldrich, 2020; Carl Roth, 2021b; Carl Roth, 2021a; Carl Roth, 2022a; Carl Roth, 2022b; Sigma Aldrich, 2022).

<sup>g</sup>(Wang et al., 2021); <sup>h</sup>(Donnaperna et al., 2009; González et al., 2015); <sup>i</sup>(Pan et al., 2021); <sup>d</sup>(Abramian and El-Rassy, 2009); <sup>e</sup>(Saad et al., 2010; Saleh and Al-Absi, 2017); <sup>f</sup>(Crandon et al., 2020); <sup>g</sup>(EPA, 2023a); <sup>h</sup>(EPA, 2023b); <sup>i</sup>(EPA, 2023c); <sup>b</sup>value ranges extracted from all studies cited in Supplementary Material; <sup>h</sup>(Zaghouane-Boudiaf et al., 2012); <sup>1</sup>(Federal Institute for Occupational Safety and Health, 2021); <sup>m</sup>(Li et al., 2009); <sup>n</sup>(Pérez-Urquiza et al., 2000).

aromatic rings and functional groups bound to the rings. The hydrophobicity and the spatial dimensions of anionic azo dyes influence the adsorption process and depend on the distance between the most distant atoms in the dye molecule, water solubility, molecular weight, and pK<sub>a</sub> (Blachnio et al., 2018; Al-Amrani et al., 2022). For further discussion, the characteristics of the five azo dyes, CR, RB5, MO, OII, and MR, are shown in Table 1, which includes their molecular structure, molecular weight, water solubility, pK<sub>a</sub>, log K<sub>OW</sub>, and λ<sub>max</sub> value, which is relevant in assessing their probability of being successfully removed from textile wastewater by adsorption.

CR shows a linear symmetry and contains two chromophore groups (-N=N-) attached to a naphthalene and benzene ring. Furthermore, a sulfonate (-SO<sub>3</sub>Na) and amino group (-NH<sub>2</sub>) are attached to each naphthalene ring. The sulfonate groups dissociate in water and are negatively charged in acidic conditions (Du et al., 2014; S; Liu et al., 2014). RB5, also known as remazol black B, is an anionic, reactive diazo dye. Reactive dyes are typically azo-based chromophores combined with different reactive groups that can form covalent bonds between dye and textile fibers (Eren and Acar, 2006). Like CR, the structure of RB5 is symmetrical and contains two chromophore groups (-N=N-). The two azo groups are attached to

a naphthalene ring in the center of RB5. Four functional groups are attached to the naphthalene ring, two sulfonate ( $-\text{SO}_3\text{Na}$ ) groups, one amino ( $-\text{NH}_2$ ), and one hydroxyl ( $-\text{OH}$ ) group. Conversely, each azo group is connected to a reactive vinyl sulfone group (Greluk and Hubicki, 2010; Tanyildizi, 2011).

MO, also known as orange III or acid orange 52, is an anionic, acid monoazo dye significantly smaller than CR and RB5 (National Center for Biotechnology Information, 2022). MO contains one chromophore group ( $-\text{N}=\text{N}-$ ) attached to two benzene rings, while one has a functional sulfonate group ( $-\text{SO}_3\text{Na}$ ). OII, also known as acid orange 7, is an anionic, acid monoazo dye. Like MO, OII contains one chromophore group ( $-\text{N}=\text{N}-$ ) but is attached to one benzene and naphthalene ring. The naphthalene ring contains a hydroxyl ( $-\text{OH}$ ) group and the benzene ring a sulfonate group ( $-\text{SO}_3\text{Na}$ ). MR or acid red 2, is also an anionic, acid monoazo dye. Like MO and OII, MR contains one chromophore group ( $-\text{N}=\text{N}-$ ). The azo group is tied to two benzene rings, where one benzene ring is attached to a carboxyl ( $-\text{COOH}$ ) functional group.

RB5 possesses the biggest molecule size of all the examined azo dyes, followed by CR, OII, MO, and MR, representing the smallest molecule. A bigger molecular size could reduce the number of molecules attaching to an adsorbent surface (Wong et al., 2019). Furthermore, MO, OII, and MR only have one chromophore group and can, therefore, be classified as mono-azo dyes, whereas RB5 and CR are diazo dyes. MO, OII, and MR have more in common; they are all acid dyes, while RB5 is reactive and CR is direct. However, all five dyes are anionic, dissociating in water and forming anions (negatively charged ions). CR, RB5, MO, and OII all contain one or more sulfonate functional group(s), which could indicate similar adsorption behavior. MR is the only dye investigated that contains a carboxyl ( $-\text{COOH}$ ) functional group. Additionally, RB5 is the only dye containing a reactive vinyl sulfone group.

The investigation of water solubility,  $\log K_{\text{OW}}$ , and  $\text{pK}_a$  provided a range of values, partly due to different testing methods, which do not allow for a clear comparison. However, the high water solubility of RB5 stands out. Comparing the values of the safety data sheets, OII seems to be very soluble, CR soluble, while MO and MR appear to be poorly soluble in water. The very negative  $\log K_{\text{OW}}$  of RB5 goes along with the reported high water solubility and implies hydrophilic behavior. The relatively high  $\log K_{\text{OW}}$  value of MR indicates that this dye is hydrophobic, i.e., poorly soluble in water. Similarly, the  $\log K_{\text{OW}}$  of CR suggests hydrophobicity, which could contribute to a higher adsorption rate. For MO and OII, it is impossible to assume based on their wide value span.

## 4 Removal of azo dyes by adsorption

In all publications, adsorption studies were performed as laboratory tests, including batch and/or column tests. The studies utilized a range of adsorbents, including both commercial sorption materials as well as materials that were developed or manufactured in-house. Overall, the studies focused on developing adsorbents based on natural materials. The analyses primarily focused on different initial dye concentrations, adsorbent dosages, pH values,

and temperatures. It is acknowledged that additional parameters, such as the stirring rate, particle size, or the surface area, were also studied in the reviewed papers. However, these parameters are not the focus of the presented study.

### 4.1 Adsorption materials

The studies investigated different adsorption materials based on carbon-based materials, e.g., fly or bottom ash, natural or modified biomass, biochar, ion exchangers (modified or unmodified), magnetic substances, and metal-organic frameworks (see Table 2). As the publications show, materials are often modified to improve the properties of adsorption materials or physical performance. Physical treatment methods, such as heating and autoclaving, and chemical processes, like pre-treatment with acids, alkalis, and organic chemicals, have been reported.

An overview of experimental parameters, optimal testing conditions, used isotherm and kinetic models, and thermodynamic parameters for all five azo dyes is listed in Supplementary Tables S1–S5.

### 4.2 Effect of initial dye concentration

The initial dye concentration has a significant impact on the effectiveness of removing azo dyes from an aqueous solution. Therefore, the effect of increasing initial dye concentration on the adsorption capacity and the percentage of dye removal (% DR) in the different studies was investigated in equilibrium. Supplementary Tables S1–S5 give a detailed overview of each investigated study's observed initial dye concentration.

Overall, 21 studies investigated the effect of increasing initial dye concentration on % DR, and 49 studies tested the effect of it on adsorption capacity. In summary, increasing the initial dye concentration led to an increase in adsorption capacity in 93.9% and a decrease in adsorption capacity in 6.1% of the studies. 64% studies for CR, 63% studies for RB5, 60% studies for MO, 91% for OII, and 80% studies for MR observed that an increase in initial azo dye concentration led to an increase in adsorption capacity. For example, the adsorption of OII on modified brown macroalgae showed an increase in adsorption capacity from 20.3 to 45.5 mg/g when the initial dye concentration was elevated from 30 to 90 mg/L (Kousha et al., 2012). Similarly, the adsorption capacity of CR onto an adsorbent made of graphene oxide/chitosan fibers with etched-off silica nanoparticles (GO/CS/ETCH) increased from 32.6 to 221 mg/g when increasing initial dye concentration from 20 to 200 mg/L (Du et al., 2014). Initial dye concentration provides the required driving force (concentration gradient) to overcome the mass transfer resistance to transfer dye molecules from the bulk solution to the adsorbent surface (Vimonses et al., 2009; Mohammadi et al., 2011). Therefore, an increase in initial dye concentration intensifies the concentration gradient, enhancing the diffusion rate and number of dye molecules on the adsorbent surface, which ultimately increases the adsorption capacity (Vimonses et al., 2009; Ip et al., 2010; Mohammadi et al., 2011; Kousha et al., 2012; Mu and Ma, 2021). Additionally, higher initial dye concentration may lead to enhanced interactions, where the

TABLE 2 Overview of the selected studies and materials for CR, RB5, MO, OII, and MR adsorption.

Adsorption material	Azo dye	Reference
<i>Phragmites australis</i> activated carbon (PAAC)	MO	Chen et al. (2010)
Bottom ash	OII	Gupta et al. (2006)
Bottom ash	MO	Mittal et al. (2007)
Fly ash	RB5	Eren and Acar (2006)
Bamboo-activated carbon with impregnation <ul style="list-style-type: none"> <li>• Ratio 6 (BACX6)</li> <li>• ration 2 (BACX2)</li> </ul>	RB5	Ip et al. (2010)
Bone char	RB5	Ip et al. (2010)
Raw pinecone biomass of <i>P. radiate</i>	CR	Dawood and Sen (2012)
Acid-treated pinecone biomass of <i>P. radiate</i>	CR	Dawood and Sen (2012)
Coir pith carbon	CR	Namasivayam and Kavitha (2002)
Banana peel powder (BPP)	CR, RB5	Munagapati et al. (2018)
Eggshell powder (ESP)	MR	Rajoriya et al. (2021)
Sunflower seed shells	RB5	Osma et al. (2007)
Canola stalks	RB5, OII	Hamzeh et al. (2012)
De-oiled soya	MO	Mittal et al. (2007)
De-oiled soya	OII	Gupta et al. (2006)
Peanut hull	RB5	Tanyildizi (2011)
Spent brewery grains (SBG)	OII	Pedro Silva et al. (2004)
Biomass from the bark of hop bush <i>Dodonaea viscosa</i> plant	MR	(Gul et al., 2022),
Activated carbon from custard apple ( <i>Annona squamosa</i> ) fruit shell by H <sub>3</sub> PO <sub>4</sub> activation (AC-PO <sub>4</sub> )	MR	(Khan et al., 2018),
Waste straw powder grafted by citric acid and acrylamide (WS-CA-AM)	MO	Liu et al. (2020)
Mesoporous-activated carbon from durian seed (DSAC)	MR	Ahmad et al. (2015)
Activated bio-carbon from the residues of supercritical extraction of raspberries (RAC)	MR	Bazan-Wozniak and Pietrzak (2020)
Sludge-rice husk biochar (SRHB)	OII	Chen et al. (2019)
NaOH-modified tea biochar (B700-10)	OII	Mu and Ma (2021)
Phosphoric acid-treated sugarcane bagasse (SBC)	MR	Saad et al. (2010)
3D graphene oxide/high molecular weight chitosan (GO/HCS) composite	RB5	Lai et al. (2020)
Graphite oxide/cross-linked chitosan composite (GO-Ch)	RB5	Travlou et al. (2013)
Graphene oxide/chitosan fibers with etched-off silica nanoparticles (GO/CS/ETCH)	CR	Du et al. (2014)
Chitosan (CS)/MgO composite	MO	Haldorai and Shim (2014)
Magnetic chitosan composite (Fe <sub>3</sub> O <sub>4</sub> -CS)	MO	Chen et al. (2020)
Chitosan-grafted-polyacrylamide (CS-g-PAM)	MO	Labidi et al. (2019)
MnO <sub>2</sub> functionalized <i>Terminalia ivorensis</i> biomass (MTIB)	CR, MO	Omorogie et al. (2022)
Mesoporous carbon CMK-3 (silica material as complex template and sucrose as carbon source)	MO	Mohammadi et al. (2011)
Spent tea leaves modified with polyethyleneimine (SPL-PEI)	RB5, MO	Wong et al. (2019)

(Continued on following page)

TABLE 2 (Continued) Overview of the selected studies and materials for CR, RB5, MO, OII, and MR adsorption.

Adsorption material	Azo dye	Reference
Modified brown macroalga <i>Stoechospermum marginatum</i> (treated with propylamine; C <sub>3</sub> H <sub>9</sub> N)	OII	Kousha et al. (2012)
Polyacrylamide grafted xanthan gum and silica nanocomposite (XG-g-PAM/SiO <sub>2</sub> )	CR	Ghorai et al. (2013)
Calcined Ni/Mg/Al layered double hydroxides (NMA-LDOs)	CR	Lei et al. (2017)
N, N-dimethyl dehydroabietylamine oxide (DAAO) surfactant modified zeolite (SMZ)	CR	Liu et al. (2014)
Graphene oxide	MO	Robati et al. (2016)
Graphene oxide-NiFe layered double hydroxides (GO-NiFe-LDH)	CR, MO	Zheng et al. (2019)
Calcined MgNiAl LDH	MO	Zaghouane-Boudiaf et al. (2012)
Mesoporous carbon (MCSG60) synthesized using commercial silica gel as a template and sucrose as a carbon source	RB5	Galán et al. (2013)
Magnetic polymer multi-wall carbon nanotube (MPMWCNT)	OII	Gao et al. (2013)
Sodium bentonite	CR	Vimonses et al. (2009)
Kaolin	CR	Vimonses et al. (2009)
Titania aerogel	OII	Abramian and El-Rassy (2009)
Zeolite	CR	Vimonses et al. (2009)
Surfactant-modified zeolite by hexadecyl ammonium bromide (SMZ-HDTMA)	OII	Jin et al. (2008)
Polystyrene anion exchanger (PsAX)	MO	Pan et al. (2021)
Magnetic MnFe <sub>2</sub> O <sub>4</sub>	CR	Yang et al. (2014)
Acid acrylic resins (anion exchanger): Amberlite IRA-458	RB5	Greluk and Hubicki (2010)
Acid acrylic resins (anion exchanger): Amberlite IRA-958	RB5	Greluk and Hubicki (2010)
Pristine UiO-66 metal-organic framework (UiO-66-MOF)	MO, MR	Ahmadjokani et al. (2020)
Oxidized nanodiamond/UiO-66 hybrid nanocomposite (OND-UiO)	MR	Molavi et al. (2020)
Iron-benzenetricarboxylate (Fe(BTC) metal-organic framework	OII	García et al. (2014)
Metal-organic framework [MIL-53 (Fe)]	MR	(Yilmaz et al., 2016),
Metal-organic framework loaded on iron oxide nanoparticles [Fe <sub>3</sub> O <sub>4</sub> .MIL-100(Fe)]	MR	Dadfarnia et al. (2015)

probability of practical collision between the dye molecule and adsorbent is higher (Mohammadi et al., 2011; Kousha et al., 2012; Gul et al., 2022). In contrast, a decrease in adsorption capacity was observed in one RB5 study and two MO studies. Wong et al. (2019) investigated the adsorption of RB5 and MO on spent tea leaves modified with polyethyleneimine. They reported a decrease in adsorption capacity of RB5 from 24.8 to 6.7 mg/g and of MO from 22.2 to 1.6 mg/g when the initial dye concentration was increased from 50 to 100 mg/L. This opposite behavior can be explained by the limited number of active sites on an adsorbent, which is only able to adsorb a target amount of dye molecules, or by a possible electrostatic repulsion between a negatively charged azo dye and adsorbent (Robati et al., 2016; Wong et al., 2019).

The % DR decreased due to increasing initial dye concentration in 85.7% of the studies and showed no increase in investigated studies. Specifically, a % DR decrease was observed in three CR, four RB5, five MO, three OII, and three MR studies. The adsorption of CR on coir pith carbon demonstrated that an increase in initial dye

concentration from 20 to 80 mg/L led to a dye removal decrease from 66.5% to 30.5% (Namasivayam and Kavitha, 2002). Similarly, an adsorption study of MR on eggshell powder found a % DR decrease from 82.2% to 40.3% when increasing MR concentration from 20 to 100 mg/L (Rajoriya et al., 2021). The reason is that the number of active sites is limited to a fixed adsorbent dosage. Nearly complete coverage of binding sites on the adsorbent leads to an apparent reduction of % DR by a further increase of the initial dye concentration because dye molecules remain in the solution (Mohammadi et al., 2011; Zaghouane-Boudiaf et al., 2012; Wong et al., 2019; Zheng et al., 2019; Mu and Ma, 2021).

For some studies, the results were not as clear. The adsorption of RB5 on sunflower seed shells showed a decrease of % DR with increasing initial dye concentration in the first 30 min of the adsorption process. However, a higher % DR was observed afterward for higher initial dye concentrations (Osma et al., 2007). On the contrary, OII adsorption on a titania aerogel adsorbent started with an increase in % DR but then decreased

above 200 mg/L initial dye concentration (Abramian and El-Rassy, 2009). The adsorption of MO onto a chitosan/MgO composite showed no significant change in % DR with increasing initial dye concentration from 50 to 300 mg/L (Haldorai and Shim, 2014). Haldorai and Shim (2014) explained this by the extensive surface area of the adsorbent and the electrostatic interactions between MO and the adsorbent.

The results generally revealed that the adsorption capacity tended to increase, and the % DR decreased when the initial dye concentration was raised. However, the effect of the initial dye concentration on the adsorption process depends not only on the adsorbent dosage but also on other critical parameters, such as pH, temperature, and surface charge. The investigated studies used various experimental parameters, making a comparison of the results difficult. Too high initial dye concentration and/or too little adsorbent dosage would, for example, lead to a quick coverage of all active adsorption sites and, as a result, remaining high dissolved azo dye concentrations. Nevertheless, the outcome shows the importance of using an adequate amount of adsorbent dosage for an expected initial dye concentration. We recommend the determination of a maximum sorption capacity for the investigated adsorbent.

### 4.3 Effect of adsorbent dosage

Investigating the effect of adsorbent dosage helps to understand the effectiveness of an adsorbent and the ability of a dye to be adsorbed with minimal adsorbent dosage (Salleh et al., 2011). Applying an adequate amount of adsorbent is essential to ensure an economically viable adsorption process, as insufficient adsorbent dosage or overdosing would result in either low removal efficiency or high operation cost (Du et al., 2014). Supplementary Tables S1–S5 overview the observed adsorbent dosage in each investigated study.

Overall, 30 studies investigated the effect of increasing adsorbent dosage on % DR, and 23 tested its effect on adsorption capacity. 78.3% of the studies found a decrease in adsorption capacity with increasing adsorbent dosage, whereas the rest found an increase in adsorption capacity.

Specifically, five studies for CR, three for RB5, four for MO, five for OII, and one for MR observed that increased adsorbent dosage led to decreased adsorption capacity. For example, an increase in the adsorbent dosage of raw pinecone powder from 0.01 to 0.03 g led to a decrease in adsorption capacity from 13.4 to 6.28 mg/g (Dawood and Sen, 2012). Comparably, the adsorption of MO and CR on a MnO<sub>2</sub>/biomass micro-composite found a decrease of adsorption capacity from 230 to 2.37 mg/g and 250 to 2.42 mg/g, respectively, when increasing the adsorbent dosage from 10 to 1000 mg (Omorogie et al., 2022). Three possible explanations exist for this behavior. Firstly, a high ratio of adsorbent to the azo dye can lead to rapid superficial adsorption of the azo dye(s), resulting in a lower dye concentration in solution, decreasing the concentration gradient as the driving force for the adsorption process (Senthil Kumar et al., 2010; Dawood and Sen, 2012). Secondly, unsaturated adsorption sites derive from the increase in adsorbent dosage with fixed initial dye concentration (Hamzeh et al., 2012; Du et al., 2014; Lai et al., 2020). Consistent with the mass balance equation where adsorption capacity is inversely proportional to adsorbent mass, increasing adsorbent dosage reduces adsorption capacity, as fewer dye molecules adsorb per unit weight (Dawood

and Sen, 2012). However, this reduction in adsorption capacity does not necessarily lower % DR, which remains efficient despite higher adsorbent amounts, highlighting a distinct behavior between adsorption capacity and % DR. Thirdly, the reduction in adsorption capacity might be due to adsorbent particle clogging and aggregation, which would lead to a decrease in total adsorbent surface area and, as a result, lengthen the diffusion paths of the dye molecules (Hamzeh et al., 2012; Omorogie et al., 2022). An increase in adsorption capacity with increasing adsorbent dosage, on the other hand, was detected in two MO and OII studies, which both examined the adsorption on bottom ash and de-oiled soya (Gupta et al., 2006; Mittal et al., 2007). One MR adsorption study on an iron-based metal-organic framework loaded onto iron oxide nanoparticle adsorbent also reported the same behavior. It concluded that increased adsorbent dosage with a fixed initial dye concentration can lead to a larger adsorbent surface area, resulting in higher adsorption capacity (Dadfarnia et al., 2015).

An increase in % DR when increasing adsorbent dosage was reported in 93.3% of the studies. A decrease in % DR with increasing adsorbent dosage was reported in two studies, where the %DR initially increased with higher adsorbent dosages, reaching a peak at a certain point, before subsequently decreasing. However, these observations did not present a consistent trend across the studies. For example, a study of the adsorption of OII and RB5 on canola stalks reported a % DR increase from 41% to 51% and 41%–95%, respectively, when increasing adsorbent dosage from 2 to 10 g/L (Hamzeh et al., 2012). Similarly, MR adsorption on treated bagasse was investigated and showed a % DR increase from 67.8% to 83.2%, as the adsorbent dosage increased from 2 to 10 g/L (Saad et al., 2010). Similar to above, the increase in % DR with higher adsorbent dosage might be attributed to an increased adsorbent surface area with more active functional groups and pore volume and, thus, more available adsorption sites (Dadfarnia et al., 2015; Hamzeh et al., 2012; S; Liu et al., 2014; Vimonses et al., 2009).

Two studies, one of CR and RB5, do not have similar results. For the adsorption of CR onto a polyacrylamide grafted xanthan gum and silica nanocomposite (XG-g-PAM/SiO<sub>2</sub>), it was found that an amount of adsorbent of 50 mg resulted in a maximum dye removal of 96.4%. In contrast, a higher adsorbent dosage of up to 150 mg led to a lower % DR (Ghorai et al., 2013). Comparably, the adsorption of RB5 on a 3D graphene oxide/high molecular weight chitosan (GO/HCS) composite found an increase in % DR when increasing the adsorbent dosage to 15 mg, likely due to more available sorption sites (Lai et al., 2020). However, the % DR decreased with a further increase of adsorbent dosage beyond 15 mg, potentially due to the agglomeration of adsorbent particles (Lai et al., 2020).

Overall, the results indicated that adsorption capacity tends to decrease and % DR increases with increasing adsorbent dosage. However, the investigated studies used a variety of experimental parameters, making comparing the results difficult. Nevertheless, these results confirm the importance of using an adequate adsorbent dosage for an expected initial dye concentration.

### 4.4 Contact time

Another factor that affects the adsorption process is the contact time between the dye and the adsorbent. At the beginning of the adsorption, the removal rate is higher due to the large surface area of

the adsorbent (Al-Amrani et al., 2022). Commonly, dye adsorption increased with longer contact time until equilibrium, and the amount of azo dyes adsorbed at equilibrium represents the adsorbent's maximum adsorption capacity under the specific operating conditions (Al-Amrani et al., 2022). However, the adsorption rate decreases over time as fewer active sites are left on the adsorbent material until equilibrium is reached.

Therefore, in most studies, especially in the initial phase of the adsorption process, high adsorption rates were observed that eventually slowed down with time before reaching equilibrium. This demonstrates that at a high concentration, which is in the early stages of the cleaning (adsorption process), the "driving force" for adsorption is high. The initial rapid uptake of azo dyes by the adsorbents was explained by the high number of available adsorption sites on the surface area of the adsorbents at the beginning of the adsorption process, which become scarcer over time (Chen et al., 2010; Ghorai et al., 2013; Zheng et al., 2019). Decreasing adsorption rates, which were observed after this initial phase, could be attributed to the decrease in available adsorption sites and to the slower rate of diffusion of azo dye molecules from external adsorption sites on the surface area to internal adsorption sites since internal diffusion processes require more time to reach equilibrium (Chen et al., 2010; Ghorai et al., 2013; Du et al., 2014).

The time needed to reach equilibrium varied greatly among different studies and adsorbents. CR studies analyzed time spans between 10 min and 25 h. The equilibrium time for the investigated RB5 studies was significantly longer and varied between 30 min and 48 h. To reach equilibrium, more time is needed for RB5 than for CR. The reason for this could be that RB5 forms a covalent bond (Lewis, 2011), and, in contrast, CR is only fixed via physical forces, which means that equilibrium starts much more quickly. For MO studies, equilibrium was achieved between 5 min and 6 h. MO has a significantly smaller molecule size than CR and RB5, mirrored in the shorter equilibrium time. For OII, the equilibrium time ranged from 60 min to 24 h. The equilibrium for MR adsorption was achieved between 50 min and 22 h. Even though MR dye has the smallest molecule size, the equilibrium time in the investigated studies tended to be slightly longer than in MO studies, which could be explained by more vital forces/interactions in MO adsorption or due to differences in experimental parameters such as initial dye concentration or adsorbent dosage.

## 4.5 Effect of pH

The pH value of a solution is essential for the dye adsorption process since it determines the electrostatic charge of a dye molecule (Salleh et al., 2011). This can impact the degree of ionization, speciation, and structure of a dye as well as affect the dissociation of the functional groups and surface charge of an adsorbent and, consequently, the rate of adsorption (Vimonses et al., 2009; Salleh et al., 2011; Dadfarnia et al., 2015).

Overall, 27 studies investigated the effect of increasing solution pH on % DR, and 32 studies tested the effect of it on adsorption capacity (see also Supplementary Tables S1–S5). 71.9% of the studies observed a decrease in adsorption capacity when increasing solution pH. Likewise, 48.2% of the studies found a reduction in % DR removal due to rising solution pH. Five studies observed no change in either % DR or adsorption capacity when increasing pH. The

investigated studies did not describe an increase in adsorption capacity or % DR when increasing solution pH.

Five studies for CR, two for RB5, seven for MO, five for OII, and four for MR observed that an increase in the initial pH of the solution led to decreased adsorption capacity. For example, the adsorption of RB5 and CR on banana peel powder showed a maximum adsorption capacity at pH 3 of 26.9 and 147 mg/g, respectively, which decreased significantly when increasing pH to 10 (Munagapati et al., 2018). Likewise, Du et al. (2014) reported that CR adsorption onto GO/CS/ETCH decreased adsorption capacity from 123.7 to 99.4 mg/g when raising pH from 3 to 10. Another study investigated the effect of pH between 1 and 10 on MR adsorption on hopbush bark and found that the maximum adsorption capacity of 34 mg/g occurred at pH 1 and was reduced to 2.5 mg/g at pH 9 (Gul et al., 2022).

A decrease in % DR was observed in two CR, four RB5, four MO, two OII studies, and one MR study. The adsorption of RB5 on a graphene oxide/cross-linked chitosan composite, for instance, demonstrated a % DR of 86% at pH 2, which decreased to 36% at pH 12 (Travlou et al., 2013). Similarly, CR was almost entirely removed at pH 3 by a zeolite adsorbent but continuously decreased to less than 80% removal at pH 11 (Vimonses et al., 2009). On the contrary, pH was not a critical factor for two CR and three RB5 studies, and no change in either % DR or adsorption capacity could be observed. For example, the adsorption of CR onto a MnFe<sub>2</sub>O<sub>4</sub> adsorbent showed a % DR of around 99% from pH 4 to 9 (Yang et al., 2014).

Many studies did not observe a clear trend for % DR and adsorption capacity (40.7% of the studies for % DR and 21.9% of the studies for adsorption capacity). For instance, % DR of CR on Kaolin decreased only when pH was higher than 9 (Vimonses et al., 2009). Similar behavior was observed for the adsorption of RB5 on spent tea leaves for pH higher than 7 (Wong et al., 2019) and for MO adsorption on a chitosan/MgO composite for pH higher than 8 (Haldorai and Shim, 2014). The same was reported for different MR adsorption studies on activated carbon from durian seed, activated carbon from custard apple fruit shell activated by H<sub>3</sub>PO<sub>4</sub>, and phosphoric acid treated sugarcane bagasse for pH above 7, 5, and 6, respectively (Saad et al., 2010; Ahmad et al., 2015; Khan et al., 2018). Omorogie et al. (2022) reported for MO and CR adsorption on a MnO<sub>2</sub>/biomass composite that maximum adsorption was attained at pH 3, and it decreased to minimum adsorption capacity when rising pH up to 10 for MO and 8 for CR. However, further increase of pH to 12 led to increasing adsorption capacity (Omorogie et al., 2022).

The optimal pH for maximum CR adsorption ranged from 2 to 4 for 79% of the studies; one study showed maximum adsorption for pH below 9, the results of another study were independent of pH between 3 and 11, and one study did not investigate the effect of changing pH on adsorption. For RB5, the optimal pH was 0.5–3 in 38% of the studies. Eight RB5 studies did not investigate the effect of changing pH; one study found that the optimal pH for RB5 adsorption was at pH 7, and the results of another study were independent of pH with values between 2–10. The optimal pH for MO adsorption was in the range of 1–5 in 80% of the studies. Two studies found the optimal pH between 6 and 9. The optimal pH for maximum OII adsorption extended from 1 to 4.5 for eight studies. The other three studies did not test the effect of

pH on adsorption. For MR, the optimal pH was 1–5 in 80% of the studies. One study found it at pH 6, and another reported the highest % DR between pH 2–6.

In conclusion, 53 studies tested the effect of changing the pH of the solution on the adsorption process, and 92.5% found that the adsorption of the five azo dyes was favored at an acidic pH between 1 and 5. In contrast, higher pH resulted in lower adsorption, which agrees with the previously reported  $pK_a$  values of the azo dyes. While the values differed for the various dyes, most said  $pK_a$  values were below or around 5, suggesting that if pH was higher than 5, the functional groups of the azo dyes were deprotonated. Hence, less acidic or basic conditions could weaken forces, reduce the attraction, or even lead to repulsion between dye molecules and adsorbent (Travlou et al., 2013). Other review studies, such as Salleh et al. (2011), have reported similar findings for the adsorption of anionic dyes by different agricultural solid wastes. They found that low solution pH resulted in a more positively charged adsorbent surface, which increased negatively charged anionic dye adsorption (Salleh et al., 2011).

The results suggest that electrostatic attraction was a vital adsorption mechanism. Nevertheless, many studies did not report a clear trend with changing pH, suggesting that other interactions were also involved in the adsorption process of azo dyes.

## 4.6 Effect of temperature

Various textile dye effluents have relatively high temperatures (Dawood and Sen, 2012), which could affect the dye adsorption rate and the adsorption equilibrium (Salleh et al., 2011; Dadfarnia et al., 2015). Overall, 38 studies investigated the effect of increasing temperature on adsorption capacity, and five studies tested the impact of it on % DR (see also Supplementary Tables S1–S5). 60.5% observed an increase in adsorption capacity with increasing temperature, whereas 31.6% reported a decrease in adsorption capacity.

Seven studies for CR, six for RB5, three for MO, three for OII, and four for MR observed that an increase in temperature led to a rise in adsorption capacity, indicating that adsorption was favored at higher temperatures. The adsorption of MR on activated carbon from durian seed, for instance, reported an adsorption capacity increase from 314 mg/g at 30°C to 350 mg/g at 60°C (Ahmad et al., 2015). Similarly, the adsorption of CR on calcined Ni/Mg/Al layered double oxide (NMA-LDO) showed an increase in adsorption capacity with increasing temperature from 1111 mg/g at 20°C to 1385 mg/g at 40°C (Lei et al., 2017). Additionally, the adsorption of CR and RB5 on banana peel powder reported an increase in adsorption capacity from 21.2 to 49.2 mg/g for RB5 and 112–165 mg/g for CR when elevating the temperature from 25°C to 45°C (Munagapati et al., 2018).

Contrarily, in four CR, four MO, three OII studies, and one MR study, a decrease of adsorption capacity with increasing temperature was reported, indicating that adsorption was favored at lower temperatures. For example, the adsorption capacity of OII on sludge-rice husk biochar decreased from 42.1 to 36.2 mg/g when increasing the temperature from 25°C to 45°C (Chen et al., 2019). Similar behavior was observed for MR adsorption on a metal-organic framework. The adsorption capacity decreased from 184 mg/g at 25°C to 163 mg/g at 45°C (Yilmaz et al., 2016).

The % DR was higher with increasing temperature in two out of five cases and decreased in two. In particular, the % DR increased in one MO and MR study. The % DR of MR on eggshell powder increased slightly from 82.2% at 25°C to 85.3% at 55°C (Rajoriya et al., 2021). Contrarily, the % DR decreased in one MO study and one OII study. Wong et al. (2019) reported, for example, that the % DR of MO on modified spent tea leaves reduced from 88.1% at 45°C to 61% at 60°C. They also studied the adsorption of RB5 on the same adsorbent and found that the % DR of RB5 was nearly constant over the whole tested temperature range (Wong et al., 2019). Other studies, one for RB5, one for MO, and two for OII, observed an increase in adsorption capacity only until 35°C (308 K) or 30°C, but a decrease for temperatures higher than those (Pedro Silva et al., 2004; Greluk and Hubicki, 2010; Gao et al., 2013; Chen et al., 2020).

On the one hand, an increase in adsorption capacity or % DR with increasing temperature might be attributed to increased surface activity and kinetic energy of the adsorbent particles due to the temperature rise (Ahmad et al., 2015; Munagapati et al., 2018), which might increase the collision frequency between adsorbents and dyes, leading to enhanced adsorption (Munagapati et al., 2018; Omorogie et al., 2022). Besides that, an increase in temperature might also increase the solubility and mobility of the dye molecules, leading to stronger interactions between dye molecules and solvent as well as an increase in diffusion rate (Salleh et al., 2011; Dawood and Sen, 2012; Ghorai et al., 2013; Lei et al., 2017; Wong et al., 2019). Moreover, at elevated temperatures, possible swelling effects within the internal structure of the adsorbent were reported, which could enable further penetration of large dye molecules and, therefore, increase adsorption (Dawood and Sen, 2012; Ghorai et al., 2013).

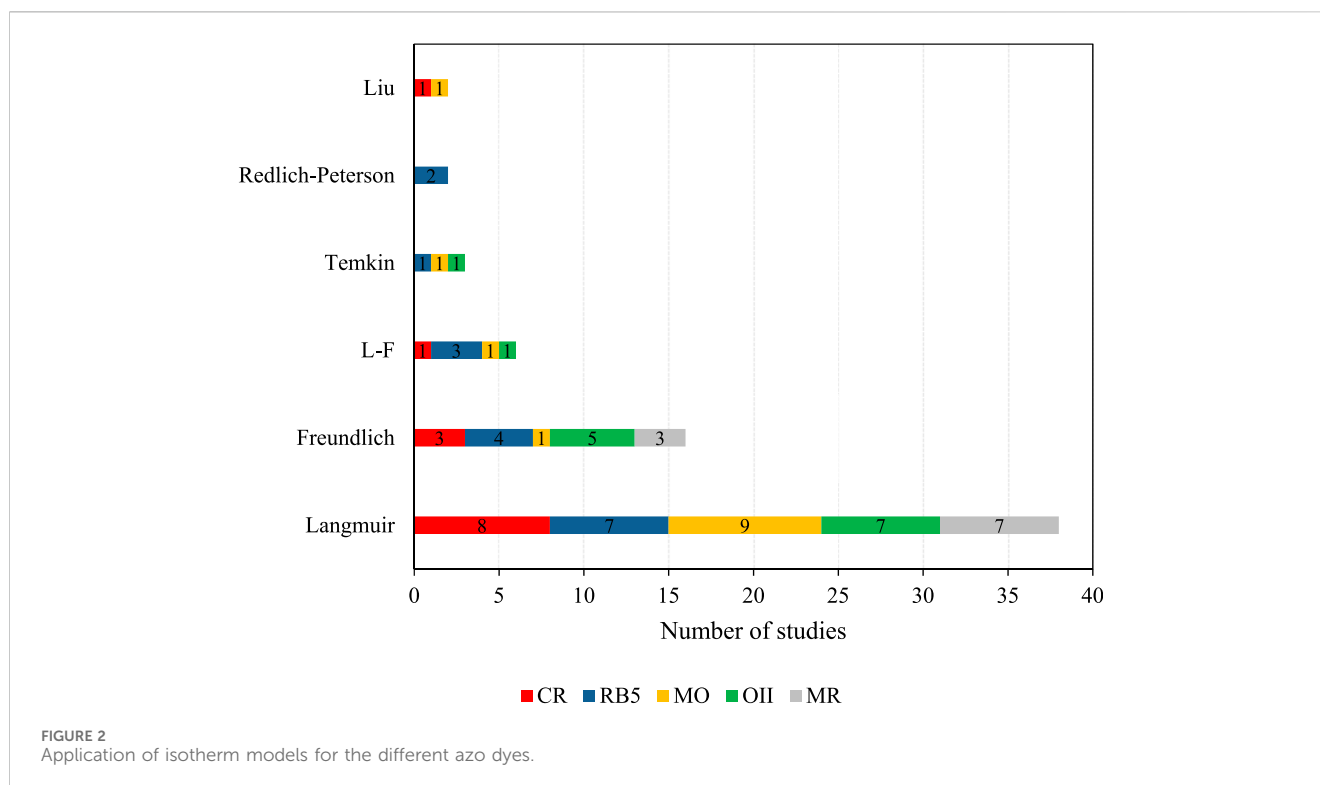
On the other hand, high temperatures leading to a decrease in adsorption capacity or % DR might be caused by a reduction of surface activity or by desorption due to the higher mobility of dye ions (Ghorai et al., 2013; Chen et al., 2020). Additionally, higher temperatures might weaken physical interactions between dye molecules and adsorption sites (Chatterjee et al., 2007; Vimonses et al., 2009).

## 4.7 Models

### 4.7.1 Isotherm models

Adsorption isotherms describe how an azo dye interacts with an adsorbent and indicate its adsorption capacity (Salleh et al., 2011). Supplementary Tables S1–S5 give a detailed overview of the isotherm model, which best describes the adsorption process in the investigated studies, based on the highest linear regression correlation coefficient  $R^2$ . 62 studies examined the applicability of different isotherm models. Five studies found that two models were equally applicable.

As illustrated in Figure 2, 61.3% of the studies found that the Langmuir isotherm model best described the adsorption process. Specifically, this was the case for eight CR, seven RB5, nine MO, seven OII, and 7 MR studies. The  $R^2$  values, indicating how well the experimental data was fitted to the model, ranged from  $R^2 = 0.994$ –1 for CR,  $R^2 = 0.94$ –0.998 for RB5,  $R^2 = 0.801$ –0.999 for MO,  $R^2 = 0.994$ –0.998 for OII, and  $R^2 = 0.990$ –0.999 for MR. Langmuir isotherm suggests monolayer adsorption on a homogeneous surface.

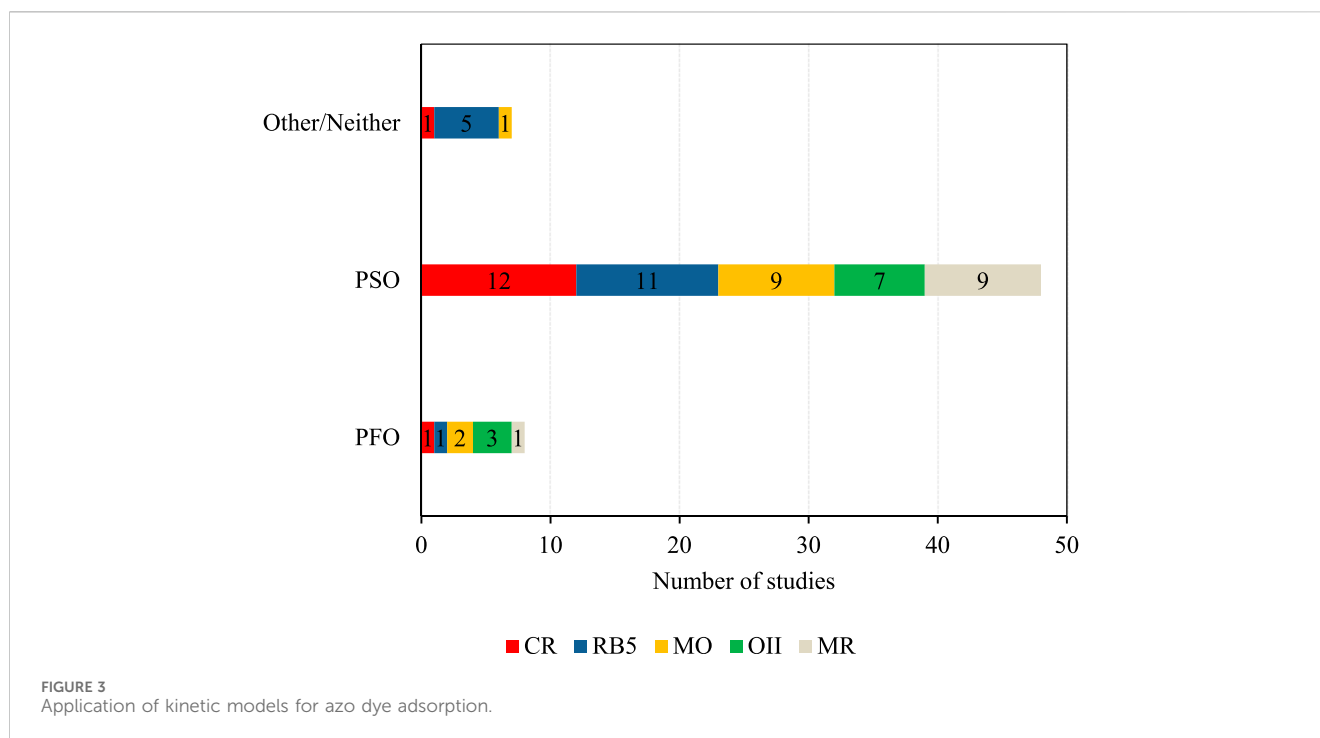


For CR, the theoretically calculated maximum monolayer adsorption capacity of the reviewed studies according to Langmuir ranged from 3.77 mg/g for zeolite (Vimonse et al., 2009) to 1250 mg/g for NMA-LDO adsorbent (Lei et al., 2017). High adsorption capacity of 294, 209, and 165 mg/g were also achieved for adsorption on GO/CS/ETCH, XG-g-PAM/SiO<sub>2</sub>, and banana peel powder, respectively (Ghorai et al., 2013; Du et al., 2014; Munagapati et al., 2018). For RB5, the maximum monolayer adsorption capacity varied from 32.8 mg/g for adsorption on canola stalks (Hamzeh et al., 2012) to 1724 mg/g for adsorption on acid acrylic resins (Greluk and Hubicki, 2010). High adsorption capacity of 639 and 55.6 mg/g were also reported for RB5 adsorption on GO/HCS and peanut hull, respectively (Tanyildizi, 2011; Lai et al., 2020). For MO, the maximum AC, according to Langmuir, was found to range from 13.4 mg/g for bottom ash (Mittal et al., 2007) to 3053 mg/g for adsorption on waste straw powder grafted by citric acid and acrylamide (WS-CA-AM) (Liu et al., 2020). While the adsorption capacity of 3053 mg/g seems relatively high, it should be noted that the  $R^2$  value in this study was only 0.801, indicating that the experimental data could not ideally be fitted to the model. Therefore, the information is not scientifically meaningful. High adsorption capacity of 455, 238, 639, and 375 mg/g were also achieved for MO adsorption on UiO-66 metal-organic framework (UiO-66-MOF), *Phragmites australis* activated carbon, magnetic chitosan composite, and calcined MgNiAl layered double hydroxide (LDH), respectively (Chen et al., 2010; Zaghouane-Boudiaf et al., 2012; Ahmadijokani et al., 2020; Chen et al., 2020). For OII, maximum monolayer adsorption capacity ranged from 2.74 mg/g for de-oiled soya as adsorbent (Gupta et al., 2006) to 435 mg/g for OII adsorption onto iron-benzene dicarboxylate, a metal-organic framework material (García et al., 2014). High

adsorption capacity of 420, 42.1, and 67.6 mg/g were also achieved for adsorption on titania aerogel, sludge-rice husk biochar, and a magnetic polymer multi-wall carbon nanotube, respectively (Abramian and El-Rassy, 2009; Gao et al., 2013; Chen et al., 2019). For MR, the maximum adsorption capacity, according to Langmuir, varied from 1.66 mg/g for adsorption on eggshell powder (Rajoriya et al., 2021) to 625 mg/g for adsorption on an iron-based metal-organic framework loaded onto iron oxide nanoparticle (Dadfarnia et al., 2015). High adsorption capacity of 385, 435, and 560 mg/g were also achieved for adsorption of MR on UiO-66-MOF, activated carbon from custard apple fruit shell by H<sub>3</sub>PO<sub>4</sub> activation, and oxidized nanodiamond/UiO-66 hybrid nanocomposite (OND-UiO), respectively (Khan et al., 2018; Ahmadijokani et al., 2020; Molavi et al., 2020).

Experimental data to the Langmuir isotherm model suggests monolayer adsorption of the azo dye on a homogenous adsorbent surface, which was the case in most investigated studies, which means that the uptake of azo dyes on the homogeneously distributed adsorption sites, which were all energetically identical, occurred until a monolayer on the adsorbent surface was completed (Hamzeh et al., 2012; Galán et al., 2013; Chen et al., 2020).

In contrast, 16 studies (25.8%) found that Freundlich isotherm provided a better fit to their experimental data. Specifically, this was the case for three CR, four RB5, one MO, five OII, and three MR studies. The  $R^2$  values for the CR studies ranged from 0.96 to 0.988, and the  $K_F$  values from 0.52 for adsorption on zeolite (Vimonse et al., 2009) to 19.2 for raw pinecone powder (Dawood and Sen, 2012). For RB5,  $R^2$  varied from 0.94 to 0.98 and  $K_F$  from 0.0376 for adsorption on sunflower seed shells (Osma et al., 2007) to 5.75 for adsorption on powdered activated carbon (Eren and Acar, 2006). The one MO study



that followed Freundlich isotherm, MO adsorption on a polystyrene anion exchanger, reported  $R^2 = 0.998$  and  $K_F = 2.12$  (Pan et al., 2021). For OII,  $R^2$  varied from 0.968 to 0.99, and  $K_F$  from 1 to 23.6 for adsorption on bottom ash and de-oiled soya (Gupta et al., 2006) and NaOH-modified tea biochar (Mu and Ma, 2021), respectively. The  $R^2$  values for MR ranged from 0.983 to 0.999, and the  $K_F$  values from 0.00707 for adsorption on biomass from the bark of hop bush (Gul et al., 2022) to 48.4 for activated biocarbon from the residues of supercritical extraction of raspberries (Bazan-Wozniak and Pietrzak, 2020). For these studies, adsorption behavior seemed heterogeneous, suggesting that it occurred between interlayer spaces and was not restricted to forming a monolayer (Vimonses et al., 2009; Hamzeh et al., 2012).

Additionally, six studies (9.68%) reported the best fit for their data to the Langmuir-Freundlich model ( $R^2 = 0.973$ –0.999), which suggests an interaction of homo- and heterogeneous active sites, resulting in monolayer and multilayer coverage of the adsorbent surface. Finally, four studies (6.45%) correlated best with the Temkin isotherm model ( $R^2 = 0.967$ –0.99) and two each with the Redlich-Peterson (3.23%; no  $R^2$  values available) or Liu isotherm model (3.23% and  $R^2 = 0.993$ –0.996).

The results suggest that the adsorption of azo dyes tends to adsorb according to Langmuir isotherm (monolayer coverage). Hence, they show a trend, but it cannot be generalized and is material dependent. Multiple deviations from an isotherm model could have canceling effects (Metcalf and Eddy Inc, 2014).

While this review primarily focuses on linear models as indicated by  $R^2$  values, the limited discussion of chi-square values in nonlinear models highlights a potential area for future research in azo dye adsorption studies.

#### 4.7.2 Kinetic models

Kinetic models study the dynamic of an adsorption process and determine at which rate adsorption occurs (Salleh et al., 2011). Most reviewed adsorption studies applied the pseudo-first-order (PFO) and

pseudo-second-order (PSO) models to investigate the adsorption kinetics. Supplementary Tables S1–S5 give a detailed overview of the kinetic model, which best fitted (highest  $R^2$  value) the experimental data of the investigated studies. 61 studies investigated the applicability of different kinetic models. Two studies found that two different models matched their data equally well.

As illustrated in Figure 3, 78.7% found that the PSO model presented a good correlation. Specifically, this was the case for 12 CR, 11 RB5, nine MO, seven OII, and 9 MR studies. The  $R^2$  values, indicating how well the experimental data was fitted to the PSO model, ranged from  $R^2 = 0.991$ –1 for CR,  $R^2 = 0.973$ –1 for RB5,  $R^2 = 0.961$ –0.999 for MO,  $R^2 = 0.99$ –1 for OII, and  $R^2 = 0.96$ –1 for MR. A high  $R^2$  indicates a good fit with the PSO model which suggests that “the rate of adsorption of solute is proportional to the available sites on the adsorbent” (Edebali, 2019). For instance, the adsorption of CR onto NMA-LDH, RB5 on sunflower seed shells, MO on WS-CA-AM, OII on NaOH modified tea biochar, and MR on OND-UiO all revealed an excellent fit to the PSO model with  $R^2$  values of greater or equal to 0.999 (Lei et al., 2017; Q; Liu et al., 2020; Molavi et al., 2020; Mu and Ma, 2021; Osma et al., 2007).

Eight studies (13.1%) reported that the PFO model provided a better fit for the experimental data. Specifically, this was the case for one CR ( $R^2 = 0.983$ ), one RB5 (no  $R^2$  value given), one MR study, two MO (no  $R^2$  value given), and three OII ( $R^2 = 0.940$ ) studies. However, for two MO and three OII studies, only the PFO model was tested, and no comparison with the PSO model was made.

The mixed-1,2-order model was the best fit for MO and CR adsorption onto a  $MnO_2$ /biomass composite with  $R^2 = 0.998$  (Omrogie et al., 2022). For four RB5 studies, all from the same authors, neither PFO nor PSO model was found to be a good fit since the calculated adsorption capacity significantly deviated from the experimental values (Ip et al., 2010).

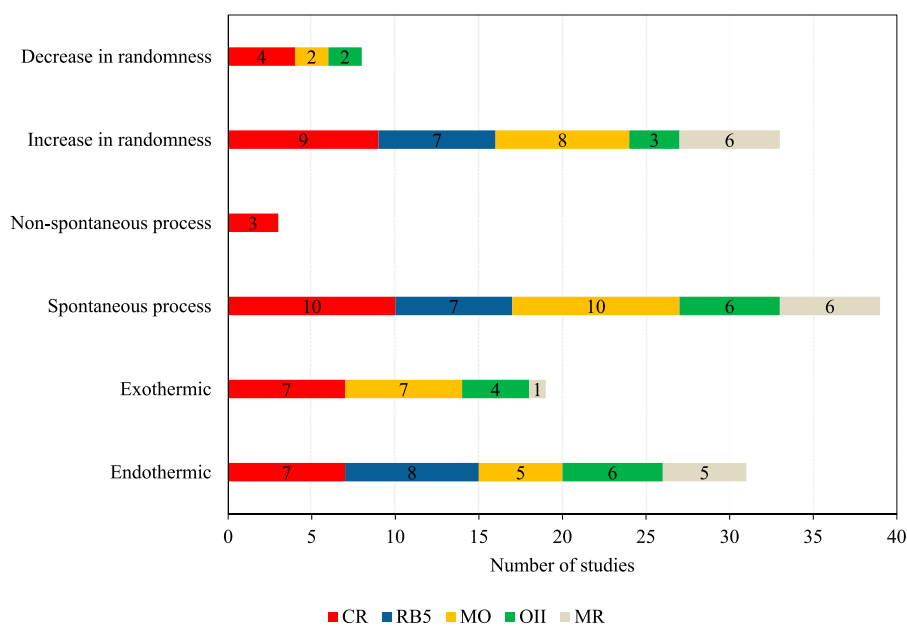


FIGURE 4  
Thermodynamic parameters investigated in the various studies of this review paper.

Adsorption processes are complex, and empirical models, such as PFO and PSO, are more descriptive than predictive (Tan and Hameed, 2017). Thus, to predict accurate behavior, kinetic experiments should be conducted under conditions similar to full-scale operation (Tan and Hameed, 2017).

Similar to isotherm models, the focus on linear regression and  $R^2$  values in kinetic models suggests a gap in the application of nonlinear methodologies, pointing to an opportunity for more comprehensive future analyses.

## 4.8 Thermodynamic parameters

Thermodynamic parameters, such as enthalpy ( $\Delta H^0$ ), entropy ( $\Delta S^0$ ), and standard Gibbs free energy ( $\Delta G^0$ ), help to further understand the nature of an adsorption process. Examining  $\Delta H^0$ ,  $\Delta S^0$ , and  $\Delta G^0$  indicates if an adsorption process is endo- or exothermic ( $\Delta H^0$ ), if it happens spontaneously ( $\Delta G^0$ ), and if it occurs randomly ( $\Delta S^0$ ). Supplementary Tables S1–S5 give a detailed overview of the thermodynamic parameters that were investigated in these studies. Enthalpy change was investigated in 50, entropy change in 41, and standard Gibbs free energy change in 42 studies.

As illustrated in Figure 4, 62% of the investigated studies highlighted the adsorption process to be endothermic ( $+\Delta H^0$ ), whereas 38% reported it as exothermic ( $-\Delta H^0$ ). The difference was described for nearly all five azo dyes.

92.9% of the studies found the adsorption process to be spontaneous ( $-\Delta G^0$ ) and feasible, implying that those systems did not require energy from external sources. Only 7.1% reported that the process was not spontaneous ( $+\Delta G^0$ ), indicating the presence of an energy barrier during the adsorption process.

Furthermore, 80.5% of studies reported an increase in randomness at the solid-liquid interface ( $+\Delta S^0$ ) during the

adsorption process, suggesting an increase in chaos and a higher degree of freedom at the adsorbate-adsorbent interface. Nevertheless, 19.5% reported a decrease in randomness at the solid-liquid interface ( $-\Delta S^0$ ), which indicates that no change in the internal structure of these adsorbents occurred, which was reported in four CR, two MO, and two OII studies.

Most studies reported that the adsorption process was endothermic and spontaneous. They showed an increase in randomness at the adsorbate-adsorbent interface, which was the case for various adsorbents and azo dyes, indicating similar behavior during the adsorption process. For instance, the adsorption of CR and RB5 on banana peel powder (Munagapati et al., 2018), of RB5 on graphite oxide/cross-linked chitosan (Travlou et al., 2013), of MO and CR on a  $\text{MnO}_2$ /biomass composite (Omorigie et al., 2022), of OII on modified tea biochar (Mu and Ma, 2021), and of MR on an iron-based metal-organic framework loaded onto iron oxide nanoparticle adsorbent (Dadfarnia et al., 2015) all reported an endothermic, spontaneous adsorption process that showed an increase in randomness at the adsorbate-adsorbent interface.

## 4.9 Synergetic or competitive interactions

Studying synergetic or competitive behavior in an adsorption process is vital to assess how well an adsorbent can perform in real wastewater conditions. Few studies investigated the synergetic or competitive adsorption behavior between different types of dyes, but none of them between various azo dyes.

For instance, Yang et al. (2014) investigated the synergetic and competitive interaction between CR and methyl blue for adsorption onto magnetic  $\text{MnFe}_2\text{O}_4$  adsorbent. They observed competitive and synergetic effects between the two dyes. In mixed solution, methyl blue adsorption capacity decreased because of competitive

interaction, whereas CR adsorption increased. The increase of CR adsorption in the presence of methyl blue was explained by the idea that CR could bind to form a 1:1 complex to already adsorbed methyl blue molecules on the adsorbent surface by hydrogen bonds and van der Waals forces, therefore providing additional adsorption sites for CR (Yang et al., 2014).

Chen et al. (2020) investigated the simultaneous adsorption of MO and methylene blue (a cationic dye) on a magnetic chitosan composite. The results indicated that, in the mixed solution, methylene blue adsorption was substantially augmented by the presence of MO molecules. Additionally, the adsorption capacity of methylene blue was proportional to the MO concentration, while MO adsorption was barely affected by the presence of methylene blue in the solution. The suggested mechanism behind this behavior was similar to the ones mentioned above. It is assumed that free MO molecules are adsorbed on the adsorbent surface by electrostatic attraction and then attract methylene blue molecules, e.g., by electrostatic attraction or  $\pi$ - $\pi$  interaction, increasing the adsorption of methylene blue (Chen et al., 2020).

Some studies also investigated the effect of salts in the solution, which would be present in real textile wastewater. Yilmaz et al. (2016) investigated MR adsorption from simulated industrial sewage. They found that the presence of salts, especially NaCl, increased the amount of MR adsorbed onto the metal-organic framework adsorbent by 6.4% compared to MR adsorption from pure MR solution (Yilmaz et al., 2016). Liu et al. (2014) investigated the effect of ionic strength on CR adsorption onto surfactant-modified zeolite. They found that ionic strength had a weak influence on the adsorption process. Nevertheless, adsorption capacity decreased slightly from 34.9 to 33.0 mg/g as the NaCl concentration increased from 0 to 1.0 mol/L. The reason for the decrease in adsorption capacity could have been competitive adsorption between chloride anions and CR (Liu et al., 2014).

## 5 Conclusion and recommendation

Many materials are available as alternatives to activated carbon, such as natural materials, biosorbents, industrial and agricultural waste, or biomass, to remove the investigated azo dyes. The adsorbents often have an excellent performance regarding removal rate or adsorption capacity. Hence, the maximum adsorption capacities vary widely, depending on the azo dye and the adsorption material. The highest maximum adsorption capacities were found for CR with 1250 mg/g for adsorption onto NMA-LDO and RB5 with 1724 mg/g for adsorption on acid acrylic resins.

In general, pH value could influence the process. In most cases, the Langmuir model and pseudo-second-order model describe the adsorption process sufficiently. However, many studies focus more on the development of an adsorption material and its characterization than on the adsorption tests.

A clear statement cannot be given based on the experimental setups. Most studies performed their experiments as batch experiments on a lab scale. No comparable standardized procedures were used, so the tests are only relative to a limited extent. Additionally, most studies investigated the adsorption of a dye from distilled water solutions. While some studies investigated

ionic strength or even simulated wastewater, more adsorption tests on real textile wastewater would be necessary to understand the effect of salts and other ingredients in textile wastewater on the adsorption of azo dyes. Furthermore, while many studies tested the adsorption of more than one azo dye, competition between different azo dyes was not frequently investigated. Additionally, there are generally fewer MR adsorption studies than the other dyes, even though it is a crucial azo dye used in the textile industry.

Generally, there needs to be more pilot or industrial-scale tests to remove azo dyes from textile wastewater. Additionally, investigations should focus more on the recovery of the materials, which was not an aspect in many papers but is essential for further practical application. Also important are the availability and the costs, which should have been investigated more.

## Author contributions

AS: Conceptualization, Data curation, Investigation, Visualization, Writing—original draft. MB: Writing—review and editing. HH: Funding acquisition, Writing—review and editing. AM: Writing—review and editing. BH: Funding acquisition, Project administration, Supervision, Validation, Writing—review and editing.

## Funding/Acknowledgement

We thank the German Research Foundation (DFG) for funding the project “Basic research on cleaning mechanisms of cementitious materials in the treatment of wastewater from the textile industry” (Project no. 495389990, HE 2413/9-1 and HI 256/6-1).

## Conflict of interest

The authors declare that the research was conducted in the absence of any commercial or financial relationships that could be construed as a potential conflict of interest.

## Publisher's note

All claims expressed in this article are solely those of the authors and do not necessarily represent those of their affiliated organizations, or those of the publisher, the editors and the reviewers. Any product that may be evaluated in this article, or claim that may be made by its manufacturer, is not guaranteed or endorsed by the publisher.

## Supplementary material

The Supplementary Material for this article can be found online at: <https://www.frontiersin.org/articles/10.3389/fenv.2024.1347981/full#supplementary-material>



- Hamzeh, Y., Ashori, A., Azadeh, E., and Abdulkhani, A. (2012). Removal of Acid Orange 7 and Remazol Black 5 reactive dyes from aqueous solutions using a novel biosorbent. *Mater. Sci. Eng. C* 32, 1394–1400. doi:10.1016/j.msec.2012.04.015
- Haque, A. N. M. A., Sultana, N., Sayem, A. S. M., and Smriti, S. A. (2022). Sustainable adsorbents from plant-derived agricultural wastes for anionic dye removal: a review. *Sustainability* 14, 11098. doi:10.3390/su141711098
- Ip, A. W., Barford, J. P., and McKay, G. (2010). A comparative study on the kinetics and mechanisms of removal of Reactive Black 5 by adsorption onto activated carbons and bone char. *Chem. Eng. J.* 157, 434–442. doi:10.1016/j.cej.2009.12.003
- Jin, X., Jiang, M., Shan, X., Pei, Z., and Chen, Z. (2008). Adsorption of methylene blue and orange II onto unmodified and surfactant-modified zeolite. *J. Colloid Interface Sci.* 328, 243–247. doi:10.1016/j.jcis.2008.08.066
- Khan, E. A., Shahjahan, and Khan, T. A. (2018). Adsorption of methyl red on activated carbon derived from custard apple (*Annona squamosa*) fruit shell: equilibrium isotherm and kinetic studies. *J. Mol. Liq.* 249, 1195–1211. doi:10.1016/j.molliq.2017.11.125
- Kousha, M., Daneshvar, E., Sohrabi, M. S., Jokar, M., and Bhatnagar, A. (2012). Adsorption of acid orange II dye by raw and chemically modified brown macroalga *Stoechospermum marginatum*. *Chem. Eng. J.* 192, 67–76. doi:10.1016/j.cej.2012.03.057
- Labidi, A., Salaberria, A. M., Fernandes, S. C. M., Labidi, J., and Abderrabba, M. (2019). Functional chitosan derivative and chitin as decolorization materials for methylene blue and methyl orange from aqueous solution. *Materials* 12, 361. doi:10.3390/ma12030361
- Lai, K. C., Lee, L. Y., Hiew, B. Y. Z., Yang, T. C.-K., Pan, G.-T., Thangalazhy-Gopakumar, S., et al. (2020). Utilisation of eco-friendly and low-cost 3D graphene-based composite for treatment of aqueous Reactive Black 5 dye: characterisation, adsorption mechanism and recyclability studies. *J. Taiwan Inst. Chem. Eng.* 114, 57–66. doi:10.1016/j.jtice.2020.09.024
- Lei, C., Zhu, X., Zhu, B., Jiang, C., Le, Y., and Yu, J. (2017). Superb adsorption capacity of hierarchical calcined Ni/Mg/Al layered double hydroxides for Congo red and Cr(VI) ions. *J. Hazard. Mater.* 321, 801–811. doi:10.1016/j.jhazmat.2016.09.070
- Lewis, D. M. (2011). "The chemistry of reactive dyes and their application processes," in *Handbook of textile and industrial dyeing. Principles, processes and types of dyes*. Editor M. Clark (United Kingdom: Woodhead Publishing), 303–364. doi:10.1533/9780857093974.2.301
- Li, G., Wang, N., Liu, B., and Zhang, X. (2009). Decolorization of azo dye Orange II by ferrate(VI)-hypochlorite liquid mixture, potassium ferrate(VI) and potassium permanganate. *Desalination* 249, 936–941. doi:10.1016/j.desal.2009.06.065
- Li, Q., Lv, C., Xia, X., Peng, C., Yang, Y., Guo, F., et al. (2022). Separation/degradation behavior and mechanism for cationic/anionic dyes by Ag-functionalized Fe<sub>3</sub>O<sub>4</sub>-PDA core-shell adsorbents. *Front. Environ. Sci. Eng.* 16, 138. doi:10.1007/s11783-022-1572-1
- Liu, Q., Li, Y., Chen, H., Lu, J., Yu, G., Möslang, M., et al. (2020). Superior adsorption capacity of functionalised straw adsorbent for dyes and heavy-metal ions. *J. Hazard. Mater.* 382, 121040. doi:10.1016/j.jhazmat.2019.121040
- Liu, S., Ding, Y., Li, P., Diao, K., Tan, X., Lei, F., et al. (2014). Adsorption of the anionic dye Congo red from aqueous solution onto natural zeolites modified with N,N-dimethyl dehydrobiethylamine oxide. *Chem. Eng. J.* 248, 135–144. doi:10.1016/j.cej.2014.03.026
- Mani, S., and Bharagava, R. (2018). "Textile industry wastewater: environmental and Health hazards and treatment approaches," in *Recent advances in environmental management*. Editor N. R. Bharagava (United States: CRC Press), 47–69.
- Metcalf and Eddy Inc (2014). *Wastewater engineering: treatment and resource recovery*. Aecom. Fifth Edition. New York, United States: McGraw-Hill Education.
- Mittal, A., Malviya, A., Kaur, D., Mittal, J., and Kurup, L. (2007). Studies on the adsorption kinetics and isotherms for the removal and recovery of Methyl Orange from wastewaters using waste materials. *J. Hazard. Mater.* 148, 229–240. doi:10.1016/j.jhazmat.2007.02.028
- Mohammadi, N., Khani, H., Gupta, V. K., Amereh, E., and Agarwal, S. (2011). Adsorption process of methyl orange dye onto mesoporous carbon material-kinetic and thermodynamic studies. *J. Colloid Interface Sci.* 362, 457–462. doi:10.1016/j.jcis.2011.06.067
- Molavi, H., Neshastehgar, M., Shojaei, A., and Ghashghaeinejad, H. (2020). Ultrafast and simultaneous removal of anionic and cationic dyes by nanodiamond/U<sub>2</sub>O<sub>3</sub>-66 hybrid nanocomposite. *Chemosphere* 247, 125882. doi:10.1016/j.chemosphere.2020.125882
- Mu, Y., and Ma, H. (2021). NaOH-modified mesoporous biochar derived from tea residue for methylene blue and orange II removal. *Chem. Eng. Res. Des.* 167, 129–140. doi:10.1016/j.cherd.2021.01.008
- Munagapati, V. S., Yarramuthi, V., Kim, Y., Lee, K. M., and Kim, D.-S. (2018). Removal of anionic dyes (reactive black 5 and Congo red) from aqueous solutions using banana peel powder as an adsorbent. *Ecotoxicol. Environ. Saf.* 148, 601–607. doi:10.1016/j.ecoenv.2017.10.075
- Namasivayam, C., and Kavitha, D. (2002). Removal of Congo Red from water by adsorption onto activated carbon prepared from coir pith, an agricultural solid waste. *Dyes Pigments* 54, 47–58. doi:10.1016/S0143-7208(02)00025-6
- National Center for Biotechnology Information (2022). PubChem compound summary for CID 23673835, methyl orange. Available at: <https://pubchem.ncbi.nlm.nih.gov/compound/Methyl-orange> (Accessed September 30, 2023).
- OHCHR (2022). About water and sanitation: OHCHR and the right to water and sanitation. Available at: <https://www.ohchr.org/en/water-and-sanitation/about-water-and-sanitation> (Accessed September 30, 2023).
- Omorogie, M. O., Agbadaola, M. T., Olatunde, A. M., Helmreich, B., and Babalola, J. O. (2022). Surface equilibrium and dynamics for the adsorption of anionic dyes onto MnO<sub>2</sub>/biomass micro-composite. *Green Chem. Lett. Rev.* 15, 51–60. doi:10.1080/17518253.2021.2018508
- Osma, J. F., Saravia, V., Toca-Herrera, J. L., and Couto, S. R. (2007). Sunflower seed shells: a novel and effective low-cost adsorbent for the removal of the diazo dye Reactive Black 5 from aqueous solutions. *J. Hazard. Mater.* 147, 900–905. doi:10.1016/j.jhazmat.2007.01.112
- Page, M. J., McKenzie, J. E., Bossuyt, P. M., Boutron, I., Hoffmann, T. C., Mulrow, C. D., et al. (2021). The PRISMA 2020 statement: an updated guideline for reporting systematic reviews. *BMJ* 372, 71. doi:10.1136/bmj.n71
- Pan, J., Zhou, L., Chen, H., Liu, X., Hong, C., Chen, D., et al. (2021). Mechanistically understanding adsorption of methyl orange, indigo carmine, and methylene blue onto ionic/nonionic polystyrene adsorbents. *J. Hazard. Mater.* 418, 126300. doi:10.1016/j.jhazmat.2021.126300
- Pang, Y. L., and Abdullah, A. Z. (2013). Current status of textile industry wastewater management and research progress in Malaysia: a review. *Clean. - Soil, Air, Water* 41, 751–764. doi:10.1002/clen.201000318
- Pedro Silva, J., Sousa, S., Rodrigues, J., Antunes, H., Porter, J. J., Gonçalves, I., et al. (2004). Adsorption of acid orange 7 dye in aqueous solutions by spent brewery grains. *Sep. Purif. Technol.* 40, 309–315. doi:10.1016/j.seppur.2004.03.010
- Pérez-Urquiza, M., Prat, M. D., and Beltrán, J. L. (2000). Determination of chromatonated dyes in water by ion-interaction high-performance liquid chromatography. *J. Chromatogr. A* 871, 227–234. doi:10.1016/S0021-9673(99)01053-5
- Rajoriya, S., Saharan, V. K., Pundir, A. S., Nigam, M., and Roy, K. (2021). Adsorption of methyl red dye from aqueous solution onto eggshell waste material: kinetics, isotherms and thermodynamic studies. *Curr. Res. Green Sustain. Chem.* 4, 100180. doi:10.1016/j.crgsc.2021.100180
- Robati, D., Mirza, B., Rajabi, M., Moradi, O., Tyagi, I., Agarwal, S., et al. (2016). Removal of hazardous dyes-BR 12 and methyl orange using graphene oxide as an adsorbent from aqueous phase. *Chem. Eng. J.* 284, 687–697. doi:10.1016/j.cej.2015.08.131
- Saad, S. A., Isa, K., and Bahari, R. (2010). Chemically modified sugarcane bagasse as a potentially low-cost biosorbent for dye removal. *Desalination* 264, 123–128. doi:10.1016/j.desal.2010.07.015
- Saleh, T. A., and Al-Absi, A. A. (2017). Kinetics, isotherms, and thermodynamic evaluation of amine-functionalized magnetic carbon for methyl red removal from aqueous solutions. *J. Mol. Liq.* 248, 577–585. doi:10.1016/j.molliq.2017.10.064
- Salleh, M. A. M., Mahmoud, D. K., Karim, W. A. W. A., and Idris, A. (2011). Cationic and anionic dye adsorption by agricultural solid wastes: a comprehensive review. *Desalination* 280, 1–13. doi:10.1016/j.desal.2011.07.019
- Senthil Kumar, P., Ramalingam, S., Senthamarai, C., Niranjana, M., Vijayalakshmi, P., and Sivanesan, S. (2010). Adsorption of dye from aqueous solution by cashew nut shell: studies on equilibrium isotherm, kinetics and thermodynamics of interactions. *Desalination* 261, 52–60. doi:10.1016/j.desal.2010.05.032
- Sigma Aldrich (2020). Safety data sheet - orange II sodium salt. Available at: <https://www.sigmaaldrich.com/DE/en/sds/aldrich/195235>.
- Sigma Aldrich (2022). Safety data sheet - reactive black 5. Available at: <https://www.sigmaaldrich.com/DE/en/sds/sial/306452> (Accessed September 30, 2023).
- Tan, K. L., and Hameed, B. H. (2017). Insight into the adsorption kinetics models for the removal of contaminants from aqueous solutions. *J. Taiwan Inst. Chem. Eng.* 74, 25–48. doi:10.1016/j.jtice.2017.01.024
- Tanyildizi, M. Ş. (2011). Modeling of adsorption isotherms and kinetics of reactive dye from aqueous solution by peanut hull. *Chem. Eng. J.* 168, 1234–1240. doi:10.1016/j.cej.2011.02.021
- Travlou, N. A., Kyzas, G. Z., Lazaridis, N. K., and Deliyanni, E. A. (2013). Graphite oxide/chitosan composite for reactive dye removal. *Chem. Eng. J.* 217, 256–265. doi:10.1016/j.cej.2012.12.008
- UN (2022). SDG 6 - ensure availability and sustainable management of water and sanitation for all. Available at: <https://sdgs.un.org/goals/goal6> (Accessed September 30, 2023).
- Vimonses, V., Lei, S., Jin, B., Chow, C. W., and Saint, C. (2009). Kinetic study and equilibrium isotherm analysis of Congo Red adsorption by clay materials. *Chem. Eng. J.* 148, 354–364. doi:10.1016/j.cej.2008.09.009
- Wang, F., Li, L., Iqbal, J., Yang, Z., and Du, Y. (2022b). Preparation of magnetic chitosan corn straw biochar and its application in adsorption of amaranth dye in aqueous solution. *Int. J. Biol. Macromol.* 199, 234–242. doi:10.1016/j.ijbiomac.2021.12.195
- Wang, S., Luo, C., Tan, F., Cheng, X., Ma, Q., Wu, D., et al. (2021). Degradation of Congo red by UV photolysis of nitrate: kinetics and degradation mechanism. *Sep. Purif. Technol.* 262, 118276. doi:10.1016/j.seppur.2020.118276

- Wang, X., Jiang, J., and Gao, W. (2022a). Reviewing textile wastewater produced by industries: characteristics, environmental impacts, and treatment strategies. *Water Sci. Technol.* 85, 2076–2096. doi:10.2166/wst.2022.088
- Wong, S., Tumari, H. H., Ngadi, N., Mohamed, N. B., Hassan, O., Mat, R., et al. (2019). Adsorption of anionic dyes on spent tea leaves modified with polyethyleneimine (PEI-STL). *J. Clean. Prod.* 206, 394–406. doi:10.1016/j.jclepro.2018.09.201
- Yang, L., Zhang, Y., Liu, X., Jiang, X., Zhang, Z., Zhang, T., et al. (2014). The investigation of synergistic and competitive interaction between dye Congo red and methyl blue on magnetic MnFe<sub>2</sub>O<sub>4</sub>. *Chem. Eng. J.* 246, 88–96. doi:10.1016/j.cej.2014.02.044
- Yilmaz, E., Sert, E., and Atalay, F. S. (2016). Synthesis, characterization of a metal-organic framework: MIL-53 (Fe) and adsorption mechanisms of methyl red onto MIL-53 (Fe). *J. Taiwan Inst. Chem. Eng.* 65, 323–330. doi:10.1016/j.jtice.2016.05.028
- Zaghouane-Boudiaf, H., Boutahala, M., and Arab, L. (2012). Removal of methyl orange from aqueous solution by uncalcined and calcined MgNiAl layered double hydroxides (LDHs). *Chem. Eng. J.* 187, 142–149. doi:10.1016/j.cej.2012.01.112
- Zheng, Y., Cheng, B., You, W., Yu, J., and Ho, W. (2019). 3d hierarchical graphene oxide-NiFe LDH composite with enhanced adsorption affinity to Congo red, methyl orange and Cr(VI) ions. *J. Hazard. Mater.* 369, 214–225. doi:10.1016/j.jhazmat.2019.02.013